International Immunology, Vol. 16, No. 1, pp. 119–129
doi: 10.1093/intimm/dxh009

Mouse CD20 expression and function

Junji Uchida[1], Youngkyun Lee[1], Minoru Hasegawa[1], Yinghua Liang[1], Alice Bradney[1], Julie A. Oliver[1], Kristina Bowen[1], Douglas A. Steeber[1], Karen M. Haas[1], Jonathan C. Poe[1] and **Thomas F. Tedder[1]**

[1]Department of Immunology, Duke University Medical Center, Durham, NC 27710, USA

Keywords: B lymphocyte, immunotherapy, knockout mouse, mAb, signal transduction

Abstract

CD20 plays a role in human B cell proliferation and is an effective target for immunotherapy. In this study, mouse CD20 expression and biochemistry were assessed for the first time using a new panel of CD20-specific mAb, with CD20 function assessed using CD20-deficient ($CD20^{-/-}$) mice. CD20 expression was B cell restricted and was initiated during late pre-B cell development. The frequency and density of CD20 expression increased during B cell maturation in the bone marrow, with a subpopulation of transitional IgM^{hi} B cells expressing higher CD20 levels than the majority of mature recirculating B cells. Transitional T1 B cells in the spleen also expressed high CD20 levels, providing a useful new marker for this B cell subset. In $CD20^{-/-}$ mice, immature and mature B cell IgM expression was ~20–30% lower relative to B cells from wild-type littermates. In addition, CD19-induced intracellular calcium responses were significantly reduced in $CD20^{-/-}$ B cells, with a less dramatic effect on IgM-induced responses. These results reveal a role for CD20 in transmembrane Ca^{2+} movement in mouse primary B cells that complements previous results obtained using human CD20 cDNA-transfected cell lines. Otherwise, B cell development, tissue localization, signal transduction, proliferation, T cell-dependent antibody responses and affinity maturation were normal in $CD20^{-/-}$ mice. Thus, mouse and human CD20 share similar patterns of expression and function. These studies thereby provide an animal model for studying CD20 function *in vivo* and the molecular mechanisms that influence anti-CD20 immunotherapy.

Introduction

CD20 is a B lymphocyte-specific cell-surface molecule involved in the regulation of transmembrane Ca^{2+} conductance and cell-cycle progression during human B cell activation (1). CD20 is first expressed by human pre-B cells in the bone marrow, predominantly after Ig heavy chain rearrangement, with expression persisting until plasma cell differentiation (2–4). A limited analysis of CD20 transcripts in mouse cell lines and tissues suggests that mouse CD20 is also B cell specific (5). Both human and mouse CD20 cDNAs encode a membrane-embedded protein with hydrophobic regions of sufficient lengths to pass through the membrane 4 times (5–8). Mouse and human CD20 are well conserved (73%) in amino acid sequence, particularly the transmembrane and long N- and C-terminal cytoplasmic domains (5). The cytoplasmic domains are serine and threonine rich with multiple consensus sequences for phosphorylation. Human CD20 is not glycosylated, but three isoforms (33, 35 and 37,000 M_r) result from the differential phosphorylation of a single protein on different serine and threonine residues (9–11).

CD20 plays a role in the regulation of human B cell activation, proliferation and Ca^{2+} transport (12,13). Antibody ligation of CD20 can generate transmembrane signals that result in enhanced CD20 phosphorylation (10), induction of c-*myc* and B-*myb* oncogene expression (14,15), induced serine/threonine and tyrosine phosphorylation of cellular proteins (16), increased CD18, CD58 and MHC class II molecule expression (17,18), and protein tyrosine kinase activation that induces B cell adhesion (19). CD20 ligation promotes transmembrane Ca^{2+} transport (13), but does not usually lead to increased intracellular calcium ($[Ca^{2+}]_i$)[3] levels (13,20,21), except after extensive cross-linking (16). Antibody binding to CD20 inhibits B cell progression from the G_1 phase into the S/G_2 + M stages of the cell cycle following mitogen stimulation, and inhibits mitogen-induced B cell differentiation and antibody secretion (12,20–22). Extensive CD20 cross-linking can also influence apoptosis (23,24). These divergent observations may be explained in part by the finding that CD20 is a component of an oligomeric complex that forms a membrane transporter or Ca^{2+} ion channel that is activated

Correspondence to: T. F. Tedder; E-mail thomas.tedder@duke.edu

Transmitting editor: S. Koyasu

Received 29 July 2003, *accepted* 3 October 2003

during cell-cycle progression (13,25–27). Despite this, B cell development and function in a line of CD20-deficient (CD20$^{-/-}$) mice is reported to be normal (28).

The majority of human B cell-lineage malignancies express CD20 (29). Because of this, anti-CD20 mAb have become an effective therapy for non-Hodgkin's lymphoma (30–37). Whether CD20 function or its membrane-embedded structure contributes most to its effectiveness as a therapeutic target remains an open issue since studies assessing *in vivo* B cell function and therapeutic mechanisms are difficult in humans. To address this, and determine whether and how CD20 regulates normal mouse B cell function and development, we have generated mAb reactive with mouse CD20 and CD20$^{-/-}$ mice. These reagents have allowed the characterization of CD20 expression in mouse and assessment of its role in mouse B cell function.

Methods

Generation of CD20$^{-/-}$ mice

DNAs encoding the 3′ end of the *Cd20* gene were isolated from a 129/Sv strain mouse DNA phage library, mapped and sequenced to identify intron/exon boundaries (Fig. 1A and B) (38). Gene targeting used a pBluescript SK-based vector (p594; David Milstone, Brigham and Women's Hospital, Boston, MA) containing a *Pst*I (exon 5) through *Eco*RV (exon 6, ~1.8 kb) DNA fragment downstream of the pMC1-HSV

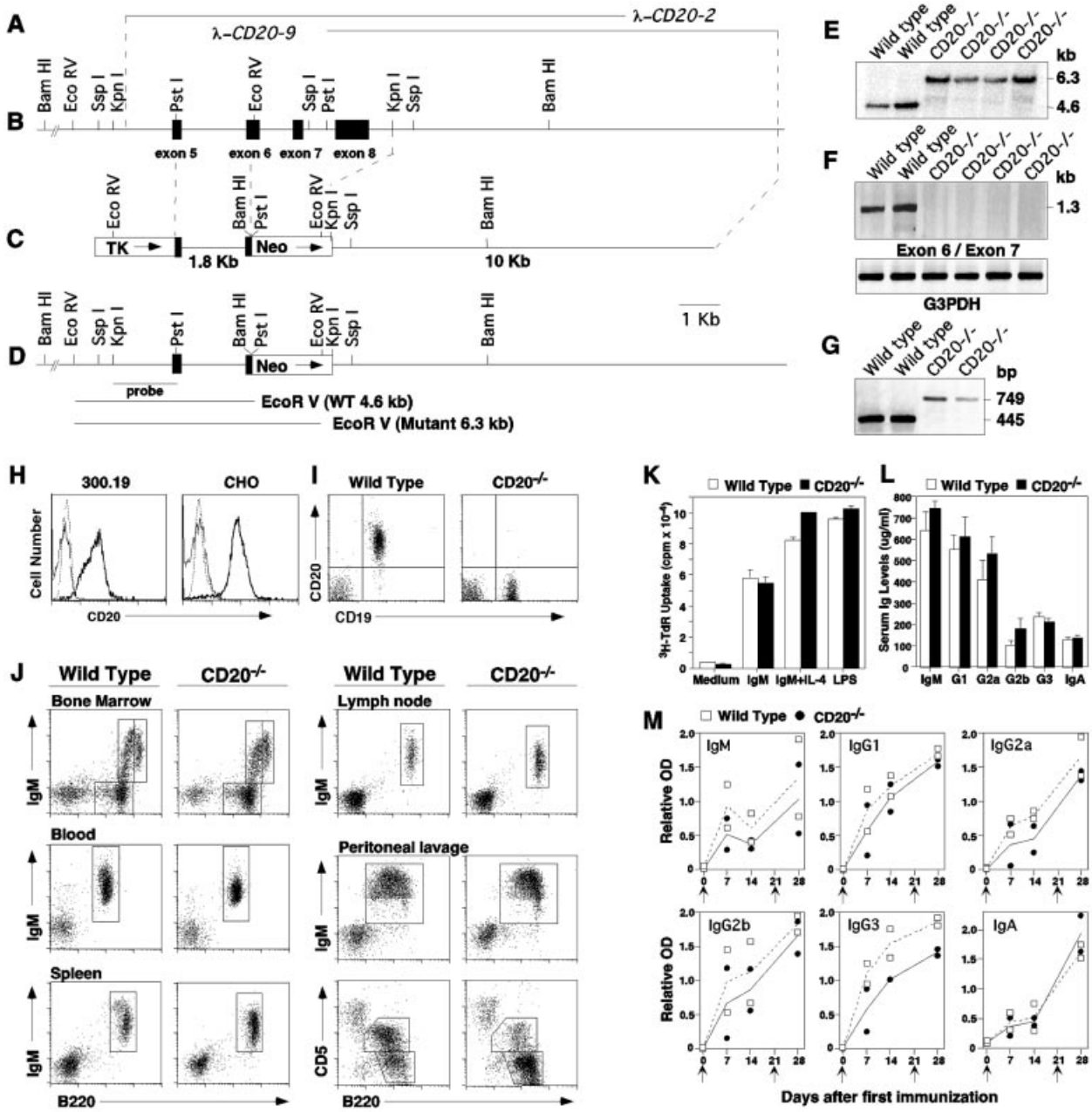

gene. An ~10 kb *Kpn*I DNA fragment was inserted downstream of the neomycin resistance (*Neo*^{r}) marker (Fig. 1C). The plasmid was linearized using a unique *Sal*I restriction site and used to transfect 129 strain-derived embryonic stem (ES) cells that were selected with G418 as described (39). Six of 115 Neo-resistant ES cell colonies carried the targeted allele (Fig. 1D). Appropriate targeting was further verified by Southern analysis of DNA digested with *Bam*HI (>12-kb fragment reduced to a 6.5-kb band), *Kpn*I (7.2 became 5.5 kb) and *Ssp*I (5.6 became 7.0 kb) using the same probe. Cells of one ES cell clone generated 80–100% chimeric male offspring that were crossed with C57BL/6 mice for seven or more generations. Heterozygous offspring were crossed to generate homozygous CD20$^{-/-}$ and wild-type littermates (Fig. 1E). In most cases, results obtained using wild-type littermates of CD20$^{-/-}$ mice and (C57BL/6 × 129)F_1 mice were identical, so the results were pooled. Spleen and peritoneal cavity subset analysis was carried out using three to 10 littermates pairs at various ages, so only comparisons between wild-type and CD20$^{-/-}$ mice are valid. Mice were housed in a specific-pathogen-free barrier facility and used at 2–3 months of age. The Animal Care and Use Committee of Duke University approved these studies.

Immunofluorescence analysis

Single-cell leukocyte suspensions were stained on ice using predetermined optimal concentrations of each antibody for 20–60 min as described (40). Cells with the forward and side light scatter properties of lymphocytes were analyzed on FACScan or FACSCalibur flow cytometers (Becton Dickinson, San Jose, CA). Background staining was determined using unreactive control mAb (Caltag, Burlingame, CA) with gates positioned to exclude 98% of the cells. Antibodies used included: CD19 mAb (MB19-1) (9–11), B220 mAb (RA3-6B2; provided by Dr Robert Coffman, DNAX, Palo, Alto, CA; Thy-1.2 (Caltag); antibodies reactive with IgM, I-A, CD5, CD11b, CD23 and CD43 (BD PharMingen, Franklin Lakes, NJ); and anti-mouse IgG3, IgM and IgD antibodies (Southern Biotechnology Associates, Birmingham, AL).

Hybridomas producing CD20-specific mouse mAb were generated by the fusion of NS-1 myeloma cells with spleen cells from CD20$^{-/-}$ mice immunized with murine CD20-green fluorescent protein (GFP) transfected 300.19 cells (41). The anti-CD20 mAb MB20-1, -2 and -14 were of the IgG1 isotype, MB20-6, -11 and -16 were IgG2a, MB20-7, -8, -10 and -18 were IgG2b, and MB20-3 and -13 were IgG3 mAb. CHO cells and the 300.19 pre-B cell line expressing mouse CD20 fused with GFP were generated by transfecting each cell line with cDNA encoding the fused proteins (5). Transfected cells were isolated by fluorescence-based cell sorting based on GFP expression.

Intracellular Ca^{2+} measurements

Changes in $[Ca^{2+}]_i$ levels were monitored by flow cytometry as described (42) after treating the cells with goat $F(ab')_2$ anti-IgM antibody (5–40 μg/ml; Cappel/ICN, Aurora, OH), anti-mouse CD19 mAb (MB19-1, 40 μg/ml), thapsigargin (1 μM; Sigma, St Louis, MO) or ionomycin (2.67 μg/ml; Calbiochem, La Jolla, CA). In some cases, EGTA (5 mM final) was added to the cell suspension, followed by the agents described above.

B cell activation assays

Spleen B cells were purified (>93% B220$^+$) by removing T cells with Thy-1.2 antibody-coated magnetic beads (Dynal, Lake Success, NY). For signal transduction studies, B cells were incubated (2×10^7/ml) in RPMI 1640 medium containing 5% FCS at 37°C for 5 min before adding $F(ab')_2$ anti-mouse IgM antibody fragments (40 μg/ml). After adding cold saline containing 400 μM EDTA and 100 μM sodium orthovanadate, the cells were then detergent lysed as described (43,44). For CD20 structural studies, B cells were surface biotinylated with EZ-Link Sulfo-NHS-Biotin (0.5 mg/ml; Pierce, Rockford, IL), then detergent lysed. Cell lysates were precleared with IgG1 mAb (1 μg) and 50 μl of a 50% suspension of Protein G–Sepharose (Amersham Biosciences, Piscataway, NJ), with proteins immunoprecipitated using 2 μg of mAb and Protein G–Sepharose. The beads were washed twice with high- and low-salt RIPA buffers, twice with PBS, boiled in sample buffer

Fig. 1. Targeted disruption of the *Cd20* gene. (A) Genomic clones encoding the 3′ end of the *Cd20* gene. (B) Intron–exon organization of wild-type *Cd20* containing exons 5–8 (filled squares). Exon numbers are based on human *CD20* structure (38). (C) Targeting vector structure. (D) Structure of the *Cd20* allele after homologous recombination, with the *Eco*RV restriction site in exon 6 deleted. (E) Southern blot analysis of genomic DNA from two wild-type and four CD20$^{-/-}$ littermates digested with *Eco*RV, transferred to nitrocellulose and hybridized with the 5′ DNA probe indicated in (D). (F) PCR amplification of genomic DNA from wild-type and CD20$^{-/-}$ littermates using primers that bind in exons 6 (5′ of *Eco*RV site) and 7. G3PDH amplification is shown as a positive control. (G) PCR amplification of cDNA generated from splenic RNA of wild-type and CD20$^{-/-}$ littermates. Each reaction mixture contained a sense primer that hybridized with sequences encoded by exon 3 and two antisense primers that hybridized with exon 6 or *Neo*^{r} gene promoter sequences. DNA amplified with exon 3 and 6 primers was 445-bp long, while exon 3 and Neo primers amplified a 749-bp fragment. (H) Reactivity of the MB20-13 mAb with CD20 cDNA-transfected (thick line) or untransfected (dashed line) 300.19 cells or CHO cells. The thin lines represent CD20 cDNA-transfected cells stained with secondary antibody alone or an isotype-control mAb. Immunofluorescence staining was visualized by flow cytometry analysis. (I) Immunofluorescence staining of splenocytes from CD20$^{-/-}$ or wild-type littermates with MB20-7 (visualized using a phycoerythrin-conjugated, anti-mouse IgG2b antibody) and anti-CD19 (FITC-conjugated) mAb with flow cytometry analysis. Quadrants delineated by squares indicate negative and positive populations of cells as determined using unreactive mAb controls. (H and I) Results are representative of those obtained with all 12 anti-mouse CD20 mAb. (J) B lymphocyte distribution in CD20$^{-/-}$ and wild-type littermates. The gated cell populations correspond to the cells described in Table 1 and represent results obtained using groups of 10 littermates. (K) Mitogen responses of CD20$^{-/-}$ B cells. Purified spleen B cells (2×10^5/well) from CD20$^{-/-}$ and wild-type littermates were cultured with anti-IgM $F(ab')_2$ antibody fragments, anti-IgM antibody plus IL-4 or LPS. Values are means (±SEM) from triplicate cultures and represent results obtained in four independent experiments. (L) Mean (±SEM) serum Ig levels for six CD20$^{-/-}$ (filled histograms) and wild-type (open histograms) littermates as measured by isotype-specific ELISA. (M) T cell-dependent humoral immune responses. Two CD20$^{-/-}$ (filled circles, solid lines) and wild-type (open squares, dashed lines) mice were immunized with DNP-KLH on days 0 and 21, with serum collected at the times indicated. Serum anti-DNP antibodies were determined by isotype-specific ELISA. Mean CD20$^{-/-}$ (solid line) and wild-type (dashed line) antibody levels are shown.

Table 1. Frequencies and numbers of B cells in CD20$^{-/-}$ mice[a]

Tissue	Phenotype	Percentage of B lymphocytes		B cell numbers ($\times 10^{-6}$)[b]		IgM levels in CD20$^{-/-}$ mice (percentage of wild-type)
		Wild-type	CD20$^{-/-}$	Wild-type	CD20$^{-/-}$	
Bone Marrow	IgM^{-} B220^{lo}	28 ± 3	27 ± 3			
	IgM^{+} B220^{lo}	14 ± 2	11 ± 1			62 ± 3**
	IgM^{+} B220^{hi}	13 ± 1	17 ± 2			93 ± 7
Blood[c]	IgM^{+} B220^{+}	63 ± 1	67 ± 2	3.0 ± 0.3	3.7 ± 0.4	69 ± 11*
Spleen	IgM^{+} B220^{+}	46 ± 4	50 ± 4	50 ± 8	66 ± 6	78 ± 6**
	IgM^{hi}B220^{lo}	4 ± 2	1 ± 1*	2.0 ± 0.3	0.8 ± 0.3*	
	CD21^{lo}HSA^{hi}	17 ± 1	22 ± 2*	7.4 ± 0.8	11.2 ± 1.4	
	CD21^{hi}HSA^{int}	14 ± 2	9 ± 1*	6.1 ± 1.2	4.5 ± 0.4	
	CD1d^{hi}CD21^{+}	5 ± 1	4 ± 1	2.6 ± 0.6	1.8 ± 0.3	
Lymph node[d]	IgM^{+} B220^{+}	21 ± 4	20 ± 1	1.0 ± 0.2	1.4 ± 0.3	88 ± 10
Peritoneum	IgM^{+} B220^{+}	73 ± 3	63 ± 5	1.1 ± 0.2	1.5 ± 0.2	84 ± 6
	CD5^{+} B220^{lo}	45 ± 3	16 ± 5**	0.8 ± 0.1	0.4 ± 0.1**	
	CD11b^{+}CD5^{-}B220^{lo}	12 ± 1	12 ± 1	0.3 ± 0.1	0.3 ± 0.2	
	CD5^{-} B220^{hi}	28 ± 1	55 ± 3**	0.5 ± 0.1	1.1 ± 0.2*	

[a]Values represent mean (± SEM) numbers or percentages of lymphocytes (based on side and forward light scatter properties) expressing the indicated cell-surface markers from three to 10 wild-type and CD20$^{-/-}$ 2-month-old littermates.
[b]B cell numbers were calculated based on total numbers of cells harvested from each tissue.
[c]Values indicate numbers of cells/ml.
[d]Values for pairs of inguinal lymph nodes.
Sample means were significantly different from wild-type littermates, *$P < 0.05$; **$P < 0.01$.

(with or without 10% 2-mercaptoethanol), electrophoresed, and transferred to nitrocellulose membranes. Blots of whole-cell lysates were probed with MB20-1 mAb, peroxidase-conjugated 4G10 antibody (Upstate Biotechnology, Lake Placid, NY), with anti-phospho-CD19 (Y513), -phospholipase Cγ (Y783), -Syk (Y525/Y526), -BTK (Y223), -Src family kinase antibodies (Cell Signaling Technology, Beverly, MA) or anti-active MAPK antibody (Promega, Madison, WI). The membranes were stripped and reprobed with a rabbit polyclonal anti-SHP-1 antibody (Upstate Biotechnology) or anti-Lyn (Lyn-44), anti-Fyn (Fyn3) and anti-ERK2 (C-14) antibodies (Santa Cruz Biotechnology, Santa Cruz, CA). Biotinylated proteins or antibodies were detected using streptavidin-conjugated horseradish peroxidase (Southern Biotechnology Associates) and an enhanced chemiluminescence kit (Pierce).

For studies of CD20 phosphorylation, primary B cells (10^7/ml) were cultured with lipopolysaccharide (LPS, *Escherichia. coli* serotype 0111:B4, 10 μg/ml; Sigma) for 48 h. Primary B cells and cell lines were then cultured in phosphate-free media for 1 h, cultured in medium containing 200 μCi/ml [^{32}P]orthophosphate (PerkinElmer, Boston, MA) for 90 min, washed, lysed, immunoprecipitated and separated by SDS–PAGE, with autoradiography as described (19,45)

Functional assays

Spleen B cell proliferation was measured by [^{3}H]thymidine incorporation as described (46). Eight-week-old mice were immunized with 2,4-dinitrophenyl-conjugated keyhole limpet hemocyanin (100 μg, DNP-KLH; Calbiochem-Novabiochem, La Jolla, CA) or were immunized twice with (4-hydroxy-3-nitrophenyl acetyl) conjugated to chicken γ-globulin (50 μg, NP_{18}-CGG) precipitated in alum as described (47). Serum DNP- and NP-specific antibody levels were measured by ELISA as described (46,48), with the relative affinity/avidity of antibody responses assessed as described (48).

Results

Generation of CD20$^{-/-}$ mice

CD20$^{-/-}$ mice were generated through targeted disruption of the *Cd20* gene in ES cells by homologous recombination. A targeting vector replaced exons encoding part of the second extracellular loop, the fourth transmembrane domain and the large C-terminal cytoplasmic domain of CD20 with a neomycin resistance gene (Fig. 1A–D). Appropriate gene targeting in ES cells was verified by Southern analysis of DNA digested with *Eco*RV, *Bam*HI, *Kpn*I and *Ssp*I. Mice homozygous for *Cd20* gene disruption were obtained at the expected Mendelian frequency by crossing heterozygous offspring of founder mice generated using targeted ES cells. Southern blot and PCR analysis of genomic DNA from homozygous offspring further verified appropriate *Cd20* gene targeting and the genomic deletion of exons 6–8 (Fig. 1E and F). Wild-type CD20 mRNA was absent in CD20$^{-/-}$ mice as confirmed by PCR amplification of cDNA generated from splenocytes of CD20$^{-/-}$ mice (Fig. 1G). As predicted, a fused *CD20-Neo^r* gene transcript was detected at low levels in CD20$^{-/-}$ mice by PCR, which translated into an aberrant CD20 peptide truncated at amino acid 157 that was fused with an 88-amino-acid peptide encoded by the *Neo^r* gene promoter sequence. Absence of cell-surface CD20 protein expression in CD20$^{-/-}$ mice was verified using a panel of 12 mouse anti-mouse CD20 mAb that were reactive with 300.19 and CHO cells transfected with CD20-GFP cDNA, but not with untransfected cells (Fig. 1H). These mAb reacted with cell-surface CD20 epitopes expressed by CD19^{+} splenocytes from wild-type mice, but not from CD20$^{-/-}$ mice (Fig. 1I). Therefore, the targeted *Cd20* gene mutation abrogated cell-surface CD20 expression.

B cell development in CD20$^{-/-}$ mice

In the 9 years since their production, CD20$^{-/-}$ mice have thrived and reproduced as well as their wild-type littermates and do not present any obvious anatomical or morphological abnormalities, or susceptibility to infections during their first year of life. CD20$^{-/-}$ mice had normal frequencies of IgM^{-} B220^{lo} pro/pre-B cells, IgM^{+} B220^{lo} immature B cells and IgM^{+} B220^{hi} mature B cells (Fig. 1J and Table 1), and normal numbers of AA4.1^{+} or HSA^{hi} B220^{lo} immature/transitional B cells in their bone marrow (data not shown). Numbers of blood, spleen and lymph node IgM^{+} B220^{+} B cells were not significantly different between CD20$^{-/-}$ mice and their wild-type littermates (Table 1).

B cell IgM expression was significantly lower in CD20$^{-/-}$ mice relative to immature and mature B cells of wild-type littermates (Table 1 and Fig. 1J). In addition, there was an ~50% reduction in numbers of IgM^{hi} B220^{lo} B cells in the spleens of CD20$^{-/-}$ littermates. Decreased numbers of IgM^{hi} B220^{lo} B cells may reflect reduced IgM expression by most B cells, but was not attributable to a loss in spleen marginal zone B cells since the number of cells with a CD1d^{hi} CD21^{+} phenotype was not significantly different between CD20$^{-/-}$ and wild-type littermates (Table 1). Likewise, numbers of transitional T1 (CD21^{lo} HSA^{hi}) and T2 (CD21^{hi} HSA^{int}) B cells, which represent recent emigrants from the bone marrow, were not reduced (Table 1). Rather, the frequency and number of T1 cells was usually higher in CD20$^{-/-}$ mice, similar to the increase in frequency of mature IgM^{+}B220^{hi} B cells observed in bone marrow of CD20$^{-/-}$ mice. Decreased numbers of IgM^{hi} B220^{lo} B cells may be attributable in part to a reduction in spleen B1 cells since there was a 64% decrease in the number of CD5^{+} B220^{lo} B1a cells within the peritoneal cavity of CD20$^{-/-}$ mice. The overall number of IgM^{+} B220^{+} B cells in the peritoneum of CD20$^{-/-}$ and wild-type littermates was similar due to an increase in the number of CD5^{-} B220^{hi} B cells (Table 1 and Fig. 1J). The number of B1b B cells (CD11b^{+} CD5^{-} B220^{lo}) was similar in CD20$^{-/-}$ and wild-type littermates (Table 1). There were no obvious differences in the size (light scatter properties) of CD20$^{-/-}$ B cells isolated from bone marrow, blood, lymph nodes or spleen when compared with B cells from wild-type littermates (not shown). An immunohistochemical analysis of spleen tissue sections revealed an otherwise normal architecture and organization of B220^{+} B cells (data not shown). Therefore, with the exception of decreased IgM expression, a reduction in the IgM^{hi} B220^{lo} B cell subset in the spleen, and low numbers of B1 cells within the peritoneal cavity, CD20 expression was not an obligate requirement for B cell development and tissue localization.

CD20$^{-/-}$ B cell function

The proliferative response of purified CD20$^{-/-}$ B cells to surface IgM ligation was comparable to wild-type B cells over a range of antibody concentrations (1–40 μg/ml; Fig. 1K and data not shown). Proliferation was also normal when the B cells were activated by LPS (Fig. 1K) over a range of concentrations (0.1–10 μg/ml, not shown) or using IL-4 (10–100 U/ml) plus anti-IgM antibody at a suboptimal (5 μg/ml) concentration. Thus, CD20 loss had no detectable effect on mitogen-induced proliferation. Normal levels of all Ig isotypes were found in sera from CD20$^{-/-}$ mice (Fig. 1L). CD20$^{-/-}$ mice also generated primary and secondary antibody responses of all isotypes that were similar to those observed in wild-type littermates following immunization with a T cell-dependent antigen, DNP-KLH (Fig. 1M). In addition, CD20$^{-/-}$ mice and their wild-type littermates generated equivalent primary and secondary IgM and IgG1 anti-NP antibody responses following immunization with NP-CGG (five mice for each group; not shown). Moreover, the affinities of primary and secondary IgG1 anti-NP antibody responses generated in CD20$^{-/-}$ mice were similar to those generated in their wild-type littermates. Therefore, CD20 function was not required for T–B cell interactions, isotype switching or affinity maturation during the generation of humoral immune responses.

CD20 expression during B cell development

Using the panel of mouse anti-mouse CD20 mAb, two mouse pre-B cell lines (300.19 and 38B9) and two T cell lines (BW5147 and BL4) failed to express CD20 cell surface protein, while the 70Z pre-B line, A20 and AJ9 mature B cell lines, and NS-1 plasmacytoma line were CD20^{+} (Figs 1H and 2A, data not shown). Similarly, CD20 was only expressed by subsets of B220^{+} cells in the bone marrow (Fig. 2B); 30 ± 3% of B220^{lo} lymphocytes were CD20^{+}, while all B220^{hi} B cells were CD20^{+} (n = 6 mice). A similar fraction of CD19^{+} B cells in the bone marrow were CD20^{+} (51 ± 2%, n = 6). Consistent with this, CD43^{+} B220^{+} pro-B cells did not express CD20, while 10 ± 1% (n = 3) of CD43^{-} IgM^{-} B220^{lo} pre-B cells expressed CD20 at low densities (Fig. 2G). All CD20^{+} pre-B cells (CD43^{-} IgM^{-} B220^{lo}) were small based on their light scatter properties, suggesting that CD20 expression was primarily initiated at or near the time of heavy chain expression. Consistent with this, the majority of immature IgM^{+} B220^{lo} B cells expressed CD20 (76 ± 9%, n = 3; fraction I, Fig. 2G). A subpopulation of immature IgM^{hi} B220^{+} (fraction II, Fig. 2G) or CD19^{lo} B cells in the bone marrow expressed CD20 at 277 ± 53% (n = 3) higher densities than mature B220^{hi} (fraction III, Fig. 2G) or CD19^{hi} B cells (Fig. 2B). Thus, CD20 is first expressed during the small pre-B cell to immature B cell transition, with CD20 expression increasing with maturation and then decreasing with entry into the mature B220^{hi} pool of recirculating B cells.

In the spleen, blood, peripheral lymph nodes and peritoneal cavity, the vast majority of IgM^{+} or B220^{+} B cells expressed CD20 (Fig. 2C–F). A small subpopulation of CD20^{hi} B220^{lo} cells was observed among blood (9 ± 1%, n = 3) and spleen (7 ± 2%, n = 3) B cells (Fig. 2C and E). The CD20^{hi} B220^{lo} B cells in the spleen were predominantly transitional T1 and T2 B cells (Fig. 2H), and are likely to represent recent emigrants from the bone marrow. T1 cells (CD21^{lo} HSA^{hi}) expressed CD20 at 139 ± 23% (n = 3) higher densities than mature B cells, while T2 cells (CD21^{hi} HSA^{hi}) expressed CD20 at 58 ± 11% (n = 3) higher densities. T1 cells (CD21^{-} CD23^{-} IgM^{hi}) and marginal zone B cells (CD21^{+} CD23^{-} IgM^{hi}), as described previously (49), also expressed CD20 at levels higher than the majority of spleen B cells (Fig. 2I). Small numbers of CD20^{-} peripheral B cells were observed in some mice, but this number was typically <2% of B220^{+} cells. In the peritoneal cavity, CD20 was expressed similarly by both CD5^{+} and CD5^{-} B cells (Fig. 2F). CD20 was not expressed at detectable levels by other subpopulations of leukocytes in any of the tissues

examined. Thus, mouse CD20 was expressed exclusively by B cells with expression initiated late during small pre-B cell maturation.

Structural characteristics of CD20

Mouse and human CD20 were compared by precipitating these molecules from surface-labeled B cell lines using the MB20-1 mAb reactive with mouse CD20 and the PB4 mAb reactive with a cytoplasmic epitope of human CD20. Mouse CD20 migrated faster than human CD20 under non-reducing conditions, but also migrated as at least two distinct molecular species with M_r of 33 and 35,000 (Fig. 3A). Under reducing conditions, mouse CD20 migrated as at least two equally represented molecular species with M_r of 40 and 42,000 (Fig. 3A). Multiple cell-surface molecules co-precipitated with mouse CD20, as occurs with human CD20 (9,16). The PB4 mAb co-precipitates molecules associated with human CD20 better than mAb that react with CD20 extracellular domains (Tedder, unpublished observations). Co-precipitation of CD20-associated molecules in mouse was not due to mAb

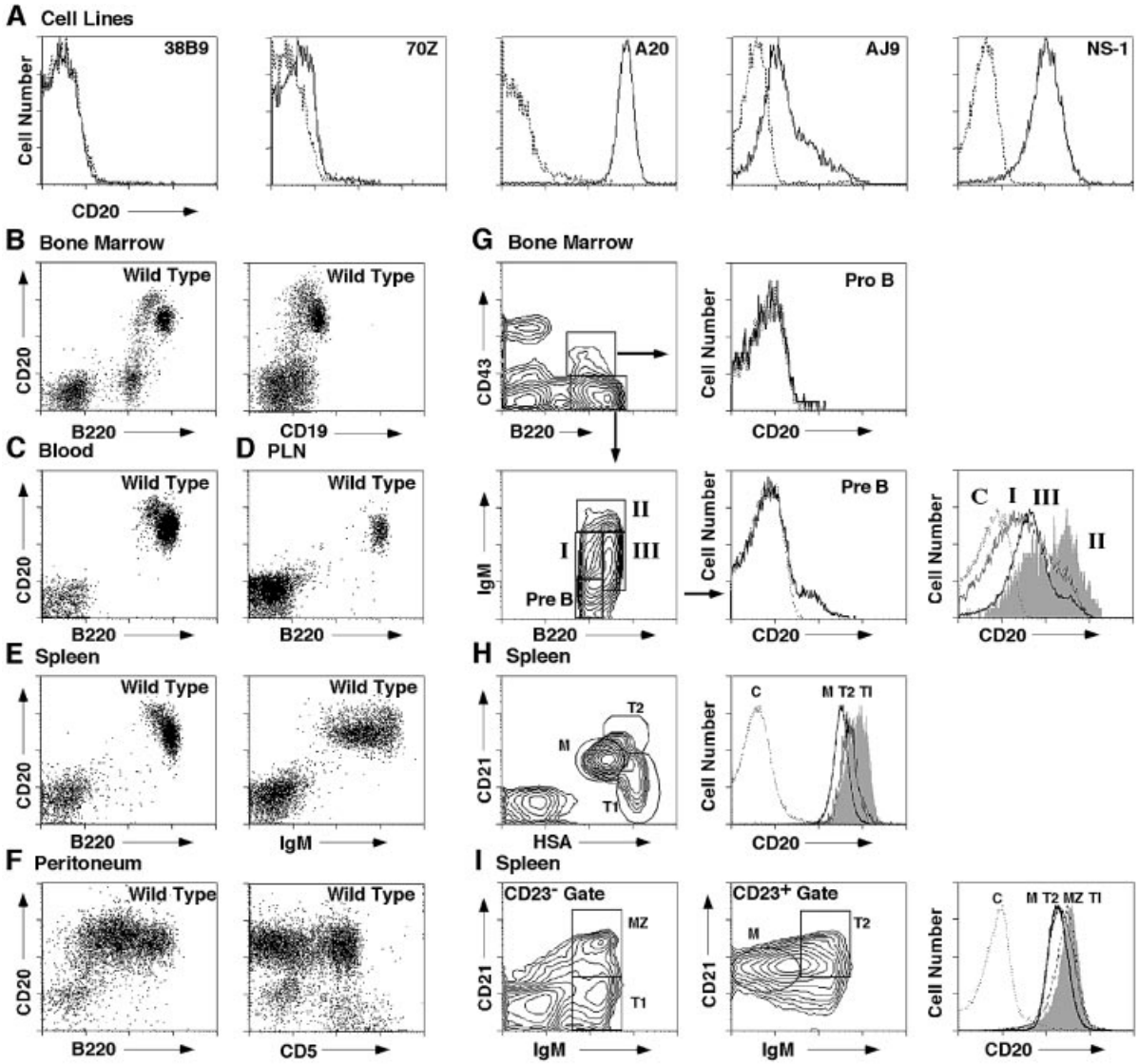

Fig. 2. CD20 expression during B cell development. (A) Immunofluorescence staining of mouse lymphoblastoid cell lines using the MB20-7 (thick line) or isotype control (dashed line) mAb. Single-cell suspensions of lymphocytes isolated from (B) bone marrow, (C) blood, (D) peripheral lymph nodes (PLN), (E) spleens and (F) peritoneal cavities of wild-type C57BL/6 mice were examined by two-color immunofluorescence staining with flow cytometry analysis. (G) CD20 expression by bone marrow B cell subpopulations assessed by four-color flow cytometry analysis. Pro-B cells were identified as CD43$^+$ B220^{lo} cells with the forward- and side-scatter properties of lymphocytes. Pre-B cells were IgM$^-$ CD43$^-$ B220^{lo} cells. Immature and mature CD43$^-$ B cells were divided into three fractions (I, II and III) based on relative IgM and B220 densities. Background fluorescence staining was assessed using isotype-matched control mAb as negative controls (C, dotted lines). (H) CD20 expression by T1, T2 or mature (M) spleen B cells as defined by relative HSA and CD21 expression densities. (I) CD20 expression by T1, T2, marginal zone (MZ) and mature (M) spleen B cells defined by CD23 expression, and relative IgM and CD21 densities. All results are representative of those obtained with three or more 2-month-old wild-type mice.

cross-reactivity since the MB20-1 mAb only reacted with mouse CD20 in western blots and CD20 or other proteins were not precipitated from lysates of CD20$^{-/-}$ B cells (Fig. 3B, data not shown). Surprisingly, mouse CD20 was not a dominant phosphoprotein in resting primary mouse B cells, anti-IgM antibody- or LPS-activated B cells, or B cell lines, even after phorbol myristate acetate (PMA) treatment (Fig. 3C), as it is in human B cells (10,50). Furthermore, PMA-induced phosphorylation of CD20 in LPS-blasts or B cell lines did not lead to a significant shift in CD20 protein M_r from the faster species to the slower species as characterizes human CD20 (10,11). Thus, mouse and human CD20 share many structural features, with some differences.

Reduced [Ca^{2+}]$_i$ responses in CD20$^{-/-}$ B cells

Despite normal B cell development in CD20$^{-/-}$ mice, splenic B220$^+$ B cells from CD20$^{-/-}$ mice generated reduced [Ca^{2+}]$_i$ responses following IgM ligation with optimal (40 μg/ml; Fig. 4A) and suboptimal concentrations (5 μg/ml; data not shown) of anti-IgM antibodies when compared with wild-type B cells. The kinetics of the immediate [Ca^{2+}]$_i$ response was not altered in CD20$^{-/-}$ B cells. However, the magnitude of the maximal [Ca^{2+}]$_i$ increase was 34 ± 4% lower ($P < 0.001$, $n = 9$) in CD20$^{-/-}$ B cells, with the level of the sustained increase observed at later time points reduced similarly. Chelation of extracellular Ca^{2+} with EGTA reduced the kinetics and magnitude of the [Ca^{2+}]$_i$ increase observed following IgM cross-linking on CD20$^{-/-}$ and wild-type B cells. The maximal magnitude of the [Ca^{2+}]$_i$ response in the presence of EGTA was 38 ± 7% lower ($P < 0.002$, $n = 7$) in CD20$^{-/-}$ B cells relative to wild-type B cells.

CD19-induced [Ca^{2+}]$_i$ responses were significantly lower (70 ± 4%, $P < 0.001$, $n = 5$) for CD20$^{-/-}$ B cells relative to wild-type B cells (Fig. 4B). Lower [Ca^{2+}]$_i$ responses did not result from decreased CD19 expression by CD20$^{-/-}$ B cells (Fig. 4D). Chelation of extracellular Ca^{2+} with EGTA mostly eliminated CD19-induced [Ca^{2+}]$_i$ responses in both wild-type and CD20$^{-/-}$ B cells. Reduced [Ca^{2+}]$_i$ responses following IgM or CD19 ligation by CD20$^{-/-}$ B cells were not likely to result from differences in internal Ca^{2+} stores or extracellular Ca^{2+} concentrations since thapsigargin- and ionomycin-induced [Ca^{2+}]$_i$ responses were slightly higher on average in CD20$^{-/-}$ B cells than in wild-type B cells (Fig. 4C, data not shown). The decrease in [Ca^{2+}]$_i$ responses in CD20$^{-/-}$ B cells is also unlikely to result from differences in genetic backgrounds. CD20$^{-/-}$ mice and their wild-type littermates were generated from 129 strain ES cells, but were backcrossed with C57BL/6 mice for at least seven generations. In control experiments, IgM-induced and CD19-induced [Ca^{2+}]$_i$ responses were similar, if not identical, for C57BL/6, (C57BL/6 × 129)F$_1$ and 129 B cells (n = 4, data not shown). Therefore, reduced [Ca^{2+}]$_i$ responses in CD20$^{-/-}$ mice were likely to result from the absence of CD20 function, rather than background differences. Since [Ca^{2+}]$_i$ responses observed following CD19 cross-linking were primarily dependent on transmembrane Ca^{2+} flux and CD19-induced [Ca^{2+}]$_i$ responses were significantly perturbed in CD20$^{-/-}$ mice, CD20 function may be particularly important for transmembrane Ca^{2+} transport.

Signal transduction in CD20$^{-/-}$ B cells

The effect of CD20 loss on B cell transmembrane signal transduction was evaluated by assessing total cellular protein tyrosine phosphorylation in purified B cells following IgM ligation. Overall levels of tyrosine phosphorylation were similar in resting splenic B cells from CD20$^{-/-}$ and wild-type littermates, although some variation was observed between

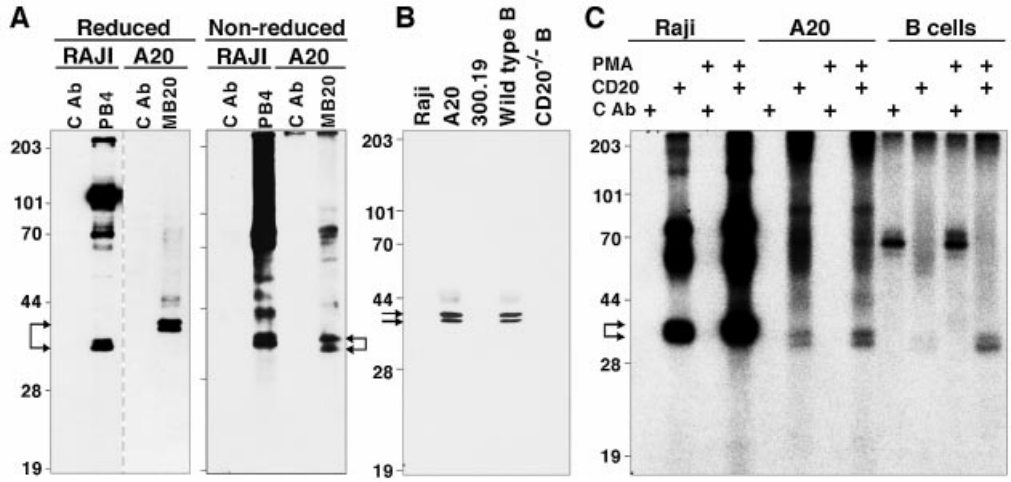

Fig. 3. Biochemical characterization of mouse CD20 and CD20$^{-/-}$ B cells. (A) CD20 immunoprecipitated (arrows) from surface-biotinylated Raji (human) and A20 (mouse) B cell lines using the PB4 (human CD20) and MB20-1 (mouse CD20) mAb respectively. Immunoprecipitations with isotype-matched control mAb (C Ab) are shown. The dashed vertical line in the reduced gel panel indicates that the results came from separate gels run in parallel. (B) Western blot analysis of CD20 expression. Lysates of Raji (1 × 10^6 cells/lane), A20 and the 300.19 B cell lines or purified mouse splenic B cells (5 × 10^6 cells/lane) were boiled under reducing conditions, separated by SDS–PAGE and transferred to nitrocellulose before probing with the MB20-1 mAb. (C) CD20 phosphorylation in primary B cells and B cell lines incubated with and without PMA. A20 cells (2 × 10^7), LPS-activated mouse splenic B cells (2 × 10^7) and Raji cells (1 × 10^7) cultured in phosphate-free media were incubated in media containing $^{32}PO_4$ for 90 min. Half of each culture was incubated with PMA (200 ng/ml) for 30 min before detergent lysis of the cells.

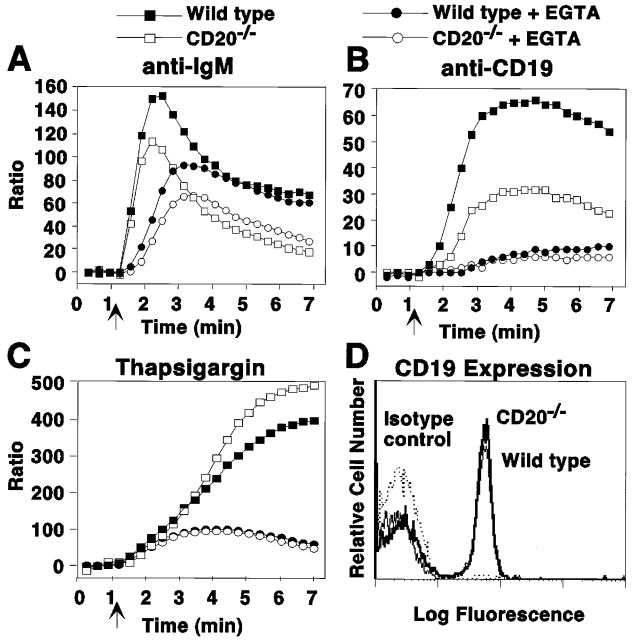

Fig. 4. Altered Ca^{2+} responses in CD20$^{-/-}$ B cells. Ca^{2+} responses induced by (A) IgM, (B) CD19 ligation or (C) thapsigargin in Indo-1-loaded B cells from CD20$^{-/-}$ and wild-type littermates. At 1 min (arrow), optimal concentrations of goat anti-IgM F(ab′)$_2$ antibody fragments, anti-CD19 mAb or thapsigargin were added, with or without EGTA present. Increased ratios of Indo-1 fluorescence indicate increased $[Ca^{2+}]_i$. Results are representative of those from at least six experiments. (D) CD19 expression by splenocytes from CD20$^{-/-}$ (thin line) and wild-type (thick line) littermates was assessed by immunofluorescence staining using phycoerythrin-conjugated anti-CD19 mAb with flow cytometry analysis. The dashed line represents staining of wild-type splenocytes with a control mAb.

B cells from individual mice in individual experiments (Fig. 5A). Protein tyrosine phosphorylation after IgM ligation was also similar in B cells from CD20$^{-/-}$ and wild-type littermates. Phosphorylation of individual signaling molecules downstream of IgM, including Lyn and other Src kinases, phospholipase Cγ, CD19, BTK, and MAP kinase, was also similar in B cells from CD20$^{-/-}$ and wild-type littermates (Fig. 5B). Thus, CD20-deficiency was unlikely to significantly alter basal or IgM-induced transmembrane signaling.

Discussion

The current study demonstrates that the vast majority of mature B cells in mice expressed cell-surface CD20 at significant levels (Fig. 2). This first time characterization of cell-surface CD20 expression in mice was made possible by generating a panel of anti-mouse CD20 mAb. The current studies confirm that mouse cell-surface CD20 expression parallels *Cd20* gene transcription (5) and human CD20 expression (2–4). CD20 was expressed after CD19 expression and was predominantly expressed at about the same time as IgM during pre-B to immature B cell development in the bone marrow (Fig. 2G). Most interesting was that CD20 expression increased with maturation and there were B cell subset-specific differences in CD20 expression density. Specifically, a subset of IgM^{hi} B cells that correspond to immature/transitional B cells (51) expressed significantly higher densities of CD20 than their less mature precursors and the mature recirculating B cells found in bone marrow (Fig. 2G). The transitional nature of these B cells was verified by the finding that T1 transitional cells found in the spleen also expressed CD20 at the highest densities, with their progeny T2 transitional cells expressing lower levels of CD20 (Fig. 2H). T1 B cells are recent immigrants from the bone marrow, which develop into T2 B cells that are found exclusively in the primary follicles of the spleen (49). Thus, human and mouse CD20 expression patterns are similar with the exception that high CD20 expression serves as an additional marker for characterizing mouse transitional B cells.

Based on the broad pattern of CD20 expression in mouse, CD20-deficiency would primarily be expected to influence immature and mature B cell function. Rather, B cell development (Fig. 1) was predominantly normal in CD20$^{-/-}$ mice, in agreement with results obtained from an independent line of CD20$^{-/-}$ mice (28). Nonetheless, CD20$^{-/-}$ mice did demonstrate some unique phenotypic and functional characteristics. Most notable was a significant reduction in transmembrane Ca^{2+} influx following CD19 or IgM ligation (Fig. 4). In addition, there was a significant reduction in cell-surface IgM expression in CD20$^{-/-}$ mice relative to their wild-type littermates (Table 1 and Fig. 1). Lower IgM expression was a characteristic feature in our CD20$^{-/-}$ mice, even as they were backcrossed with C57BL/6 mice for seven generations. Lower IgM expression was not noted in the studies of O'Keefe *et al.* (28), and this is not a characteristic of 129 B cells relative to C57BL/6 B cells. Like the CD20$^{-/-}$ mice of O'Keefe *et al.*, a reduction in peritoneal B1 cell development was found in our CD20$^{-/-}$ mice relative to their wild-type littermates (Table 1 and Fig. 2). As demonstrated by O'Keefe *et al.* (28), this deficiency may result from a polymorphic difference between the 129 and C57BL/6 strains of mice that is linked to the *Cd20* locus since CD20$^{-/-}$ and 129 strain mice had similar low frequencies of B1 cells (data not shown). Despite these differences, the activation of signaling molecules downstream of IgM was similar in CD20$^{-/-}$ mice relative to their wild-type littermates (Fig. 5). Thus, disrupted CD20 expression had selective effects on B cell development and signal transduction.

Human CD20 plays an important role in transmembrane Ca^{2+} influx (13,25–27). Consistent with this, splenic B cells from CD20$^{-/-}$ mice generated significantly reduced $[Ca^{2+}]_i$ responses following surface IgM or CD19 ligation when compared with B cells from wild-type littermates (Fig. 4). The chelation of extracellular Ca^{2+} attenuated IgM-induced $[Ca^{2+}]_i$ responses to a more significant extent, but did not eliminate $[Ca^{2+}]_i$ responses. By contrast, CD19-induced $[Ca^{2+}]_i$ responses were more dramatically inhibited by CD20 deficiency. The almost complete abrogation of CD19-induced $[Ca^{2+}]_i$ responses in the presence of EGTA suggests that CD19-induced $[Ca^{2+}]_i$ responses were primarily dependent on transmembrane Ca^{2+} influx (Fig. 4). Since CD19-induced $[Ca^{2+}]_i$ responses were most dramatically affected by CD20 loss or the chelation of extracellular Ca^{2+}, CD20 expression may predominantly contribute to conductive Ca^{2+} responses. Consistent with this, human CD20 functions either as a component of a cell-surface Ca^{2+} channel or as a direct

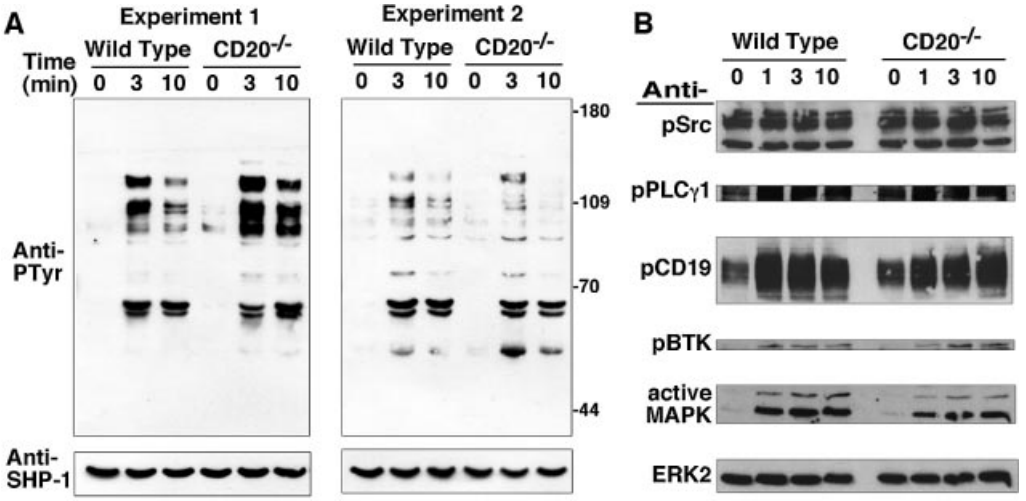

Fig. 5. Protein tyrosine phosphorylation in purified splenic B cells of CD20$^{-/-}$ and wild-type littermates. (A) B cells (2×10^7/sample) were incubated with F(ab′)$_2$ anti-IgM antibody fragments for the times shown and detergent lysed. Proteins were resolved by SDS–PAGE, transferred to nitrocellulose and immunoblotted with anti-phosphotyrosine (anti-pTyr) antibody. The blot was stripped and reprobed with anti-SHP-1 antibody as a control for equivalent protein loading. The migration of mol. wt markers (kDa) is shown for each panel. (B) Tyrosine phosphorylation of signaling molecules by CD20$^{-/-}$ B cells. Purified splenic B cells from wild-type and CD20$^{-/-}$ littermates were stimulated with F(ab′)$_2$ anti-mouse IgM antibody (40 μg/ml) for the indicated times. Detergent lysates of cells were utilized for western blot analysis with anti-phosphotyrosine antibodies to assess protein phosphorylation. The blots were subsequently stripped and reprobed with anti-ERK2 antibody to confirm equivalent protein loading between samples. All results represent those obtained in at least three separate experiments.

regulator of Ca^{2+} channel activity (1). As with all knockout mice generated in a 129 genetic background, it remains possible that decreased $[Ca^{2+}]_i$ responses in CD20$^{-/-}$ B cells result from 129 versus C57BL/6 strain differences or *Cd20*-linked 129 strain genes that function differently in a C57BL/6 genetic background. However, both IgM- and CD19-induced $[Ca^{2+}]_i$ responses in CD20$^{-/-}$ littermates were significantly less than those observed in 129 and C57BL/6 strain B cells, and this characteristic was not altered during the course of backcrossing CD20$^{-/-}$ mice with C57BL/6 mice for seven generations. Although O'Keefe *et al.* concluded that their line of CD20$^{-/-}$ mice had normal IgM-induced $[Ca^{2+}]_i$ responses, the IgM-induced $[Ca^{2+}]_i$ response shown in their study was lower in CD20$^{-/-}$ B cells than wild-type B cells and CD19-induced responses were not evaluated (28). Thus, both sets of CD20$^{-/-}$ mice may have decreased $[Ca^{2+}]_i$ responses. The incomplete blockade of $[Ca^{2+}]_i$ responses in CD20$^{-/-}$ B cells is likely to reflect the expectation that B cells express numerous Ca^{2+}-permeant channels that are structurally and functionally diverse. In addition, proteins of the CD20 or membrane-spanning 4A (MS4A) family all share significant amino sequence similarities in their transmembrane domains (52,53). Thereby, other MS4A family members may also contribute to transmembrane Ca^{2+} transport in addition to CD20, and mouse B cell lines and lymphoid tissues expressed transcripts for the majority of the currently identified MS4A family members (unpublished observations). Thus, these results confirm a role for CD20 in regulating transmembrane Ca^{2+} movement in mouse primary B cells and provide a model system that complements the previous results obtained using human CD20 cDNA-transfected cell lines (13,25–27).

While mice and humans share similar patterns of CD20 expression, there are protein sequence differences that were reflected as differences in mouse CD20 phosphorylation and migration in SDS gels (Fig. 3). Mouse CD20 contains 18 Ser/Thr residues within its proposed cytoplasmic regions with multiple consensus sequences for phosphorylation, while human CD20 contains 26 Ser/Thr residues (5). Human CD20 is significantly downstream from B cell antigen receptor-induced tyrosine kinase activation, but becomes heavily serine and threonine phosphorylated in activated B cells and cell lines (9–11). In fact, CD20 is hyperphosphorylated in hairy cell leukemia cells which also have unusually high $[Ca^{2+}]_i$ levels (54). Ubiquitous kinases such as protein kinase C, casein kinase II and calcium/calmodulin-dependent protein kinase II are likely to phosphorylate CD20 on different residues with different functional consequences (9–11,50,55,56). For example, protein kinase C-mediated phosphorylation of CD20 inactivates CD20-associated Ca^{2+} current, which may be one molecular mechanism for regulation of transmembrane Ca^{2+} conductance in B cells (13). By contrast, mouse CD20 was not hyperphosphorylated following B cell activation (Fig. 3). Divergent amino acid sequences may explain this difference. However, this implies that hyperphosphorylation may only be a small component of CD20 regulation. Alternatively, human and mouse B cells may regulate CD20 function differently. CD20 may also be regulated by other cell-surface and cytoplasmic proteins that associate with it in the membrane (9,10). Most notable in human B cells are uncharacterized cell-surface proteins of 28–30,000 and 180–200,000 M_r, and 50–60,000 M_r cytoplasmic proteins (9,57) that include serine kinases, Src family tyrosine kinases (p56/53^{lyn}, p56^{lck} and p59^{fyn}) and 75/80-kDa tyrosine phosphorylated proteins (16,58). Similar sized proteins co-precipitated with mouse CD20 (Fig. 3A). Thus, mouse CD20 is likely to form oligomeric cell-surface receptor complexes that may include MS4A family members (13).

The current demonstration that CD20 deficiency does not impart a significant functional disadvantage to B cells explains in part the evolution of CD20-deficient lymphomas following anti-CD20 immunotherapy in humans (59). With the availability of the new reagents described in this study, future experiments will be carried out to address this important, yet complex issue. Nonetheless, the current demonstration that mouse and human CD20 have similar functions and patterns of expression provides a basis for future mechanistic studies that will identify the molecular and cellular mechanisms for tumor regression, and the development of tumor resistance to anti-CD20 mAb treatment.

Acknowledgments

We thank Dr Beverley Kohler, Dr David Ord and Mr Paul Jansen for assistance in the generation and characterization of CD20$^{-/-}$ mice. This work was supported by NIH grants CA81776 and CA54464 and a Basic Science Grant from the American Arthritis Foundation.

Abbreviations

$[Ca^{2+}]_i$	intracellular calcium
CGG	chicken γ-globulin
DNP	2,4-dinitrophenyl
ES	embryonic stem
GFP	green fluorescent protein
KLH	keyhole limpet hemocyanin
LPS	lipopolysaccharide
MS4A	membrane-spanning 4A
Neo^r	neomycin resistance
NP	4-hydroxy-3-nitrophenyl acetyl
PMA	phorbol myristate acetate

References

1 Tedder, T. F. and Engel, P. 1994. CD20: a regulator of cell-cycle progression of B lymphocytes. *Immunol. Today* 15:450.
2 Stashenko, P., Nadler, L. M., Hardy, R. and Schlossman, S. F. 1980. Characterization of a human B lymphocyte-specific antigen. *J. Immunol.* 125:1678.
3 Stashenko, P., Nadler, L. M., Hardy, R. and Schlossman, S. F. 1981. Expression of cell surface markers after human B lymphocyte activation. *Proc. Natl Acad. Sci. USA* 78:3848.
4 Loken, M. R., Shah, V. O., Dattilio, K. L. and Civin, C. I. 1987. Flow cytometric analysis of human bone marrow. II. Normal B lymphocyte development. *Blood* 70:1316.
5 Tedder, T. F., Klejman, G., Disteche, C. M., Adler, D. A., Schlossman, S. F. and Saito, H. 1988. Cloning of complementary DNA encoding a new mouse B lymphocyte differentiation antigen, homologous to the human B1 (CD20) antigen and localization of the gene to chromosome 19. *J. Immunol.* 141:4388.
6 Tedder, T. F., Streuli, M., Schlossman, S. F. and Saito, H. 1988. Isolation and structure of a cDNA encoding the B1 (CD20) cell-surface antigen of human B lymphocytes. *Proc. Natl Acad. Sci. USA* 85:208.
7 Einfeld, D. A., Brown, J. P., Valentine, M. A., Clark, E. A. and Ledbetter, J. A. 1988. Molecular cloning of the human B-cell CD20 receptor predicts a hydrophobic protein with multiple transmembrane domains. *EMBO J.* 7:711.
8 Stamenkovic, I. and Seed, B. 1988. Analysis of two cDNA clones encoding the B lymphocyte antigen CD20 (B1, Bp35), a type III integral membrane protein. *J. Exp. Med.* 167:1975.
9 Tedder, T. F., McIntyre, G. and Schlossman, S. F. 1988. Heterogeneity in the B1 (CD20) cell surface molecule expressed by human B lymphocytes. *Mol. Immunol.* 25:1321.
10 Tedder, T. F. and Schlossman, S. F. 1988. Phosphorylation of the B1 (CD20) cell surface molecule expressed by normal and malignant human B lymphocytes. *J. Biol. Chem.* 263:10009.
11 Valentine, M. A., Cotner, T., Gaur, L., Torres, R. and Clark, E. A. 1987. Expression of the human B cell surface protein CD20: alteration by phorbol 12-myristate 12-acetate. *Proc. Natl Acad. Sci. USA* 84:8085.
12 Tedder, T. F., Boyd, A. W., Freedman, A. S., Nadler, L. M. and Schlossman, S. F. 1985. The B cell surface molecule B1 is functionally linked with B cell activation and differentiation. *J. Immunol.* 135:973.
13 Bubien, J. K., Zhou, L.-J., Bell, P. D., Frizzell, R. A. and Tedder, T. F. 1993. Transfection of the CD20 cell surface molecule into ectopic cell types generates a Ca^{++} conductance found constitutively in B lymphocytes. *J. Cell Biol.* 121:1121.
14 Smeland, E., Godal, T., Rudd, E., Beiske, K., Funderud, S., Clark, E. A., Pfeifer-Ohlsson, S. and Ohlsson, R. 1985. The specific induction of *myc* protooncogene expression in normal human B cells is not a sufficient event for acquisition of competence to proliferate. *Proc. Natl Acad. Sci. USA* 82:6255.
15 Golay, J., Cusmano, G. and Introna, M. 1992. Independent regulation of c-*myc*, B-*myb*, and c-*myb* gene expression by inducers and inhibitors of proliferation in human B lymphocytes. *J. Immunol.* 149:300.
16 Deans, J. P., Schieven, G. L., Shu, G. L., Valentine, M. A., Gilliland, L. A., Aruffo, A., Clark, E. A. and Ledbetter, J. A. 1993. Association of tyrosine and serine kinases with the B cell surface antigen CD20. Induction via CD20 of tyrosine phosphorylation and activation of phospholipase C-γ1 and PLC phospholipase C-γ2. *J. Immunol.* 151:4494.
17 White, M. W., McConnell, F., Shu, G. L., Morris, D. R. and Clark, E. A. 1991. Activation of dense human tonsilar B cells: induction of c-*myc* gene expression via two distinct signal transduction pathways. *J. Immunol.* 146:846.
18 Clark, E. A. and Shu, G. 1987. Activation of human B cell proliferation through surface Bp35 (CD20) polypeptides or immunoglobulin receptors. *J. Immunol.* 138:720.
19 Kansas, G. S. and Tedder, T. F. 1991. Transmembrane signals generated through MHC class II, CD19, CD20, CD39, and CD40 antigens induce LFA-1-dependent and independent adhesion in human B cells through a tyrosine kinase-dependent pathway. *J. Immunol.* 147:4094.
20 Tedder, T. F., Forsgren, A., Boyd, A. W., Nadler, L. M. and Schlossman, S. F. 1986. Antibodies reactive with the B1 molecule inhibit cell cycle progression but not activation of human B lymphocytes. *Eur. J. Immunol.* 16:881.
21 Golay, J. T., Clark, E. A. and Beverley, P. C. 1985. The CD20 (Bp35) antigen is involved in activation of B cells from the G_0 to the G_1 phase. *J. Immunol.* 135:3795.
22 Golay, J. T. and Crawford, D. H. 1987. Pathways of human B-lymphocyte activation blocked by B-cell specific monoclonal antibodies. *Immunology* 62:279.
23 Holder, M., Grafton, G., MacDonald, I., Finney, M. and Gordon, J. 1995. Engagement of CD20 suppresses apoptosis in germinal center B cells. *Eur. J. Immunol.* 25:3160.
24 Shan, D., Ledbetter, J. A. and Press, O. W. 1998. Apoptosis of malignant human B cells by ligation of CD20 with monoclonal antibodies. *Blood* 91:1644.
25 Kanzaki, M., Shibata, H., Mogami, H. and Kojima, I. 1995. Expression of calcium-permeable cation channel CD20 accelerates progression through the G_1 phase in Balb/c 3T3 cells. *J. Biol. Chem.* 270:13099.
26 Kanzaki, M., Lindorfer, M. A., Garrison, J. C. and Kojima, I. 1997. Activation of the calcium-permeable cation channel CD20 by alpha subunits of the G_i protein. *J. Biol. Chem.* 272:14733.
27 Kanzaki, M., Nie, L., Shibata, H. and Kojima, I. 1997. Activation of a calcium-permeable cation channel CD20 expressed in Balb/c 3T3 cells by insulin-like growth factor-I. *J. Biol. Chem.* 272:4964.
28 O'Keefe, T. L., Williams, G. T., Davies, S. L. and Neuberger, M. S. 1998. Mice carrying a CD20 gene disruption. *Immunogenetics* 48:125.
29 Anderson, K. C., Bates, M. P., Slaughenhoupt, B., Pinkus, G., Schlossman, S. F. and Nadler, L. M. 1984. Expression of human B

cell-associated antigens on leukemias and lymphomas: a model of human B cell differentiation. *Blood* 63:1424.
30 Kaminski, M. S., Zasadny, K. R., Francis, I. R., Milik, A. W., Ross, C. W., Moon, S. D., Crawford, S. M., Burgess, J. M., Petry, N. A., Butchko, G. M., Glenn, S. D. and Wahl, R. L. 1993. Radioimmunotherapy of B-cell lymphoma with [^{131}I]anti-B1 (anti-CD20) antibody. *N. Engl. J. Med.* 329:459.
31 Weiner, L. M. 1999. Monoclonal antibody therapy of cancer. *Semin. Oncol.* 26:43.
32 Onrust, S. V., Lamb, H. M. and Balfour, J. A. 1999. Rituximab. *Drugs* 58:79.
33 McLaughlin, P., White, C. A., Grillo-Lopez, A. J. and Maloney, D. G. 1998. Clinical status and optimal use of rituximab for B-cell lymphomas. *Oncology* 12:1763.
34 Maloney, D. G., Grillo-L'opez, A. J., White, C. A., Bodkin, D., Schilder, R. J., Neidhart, J. A., Janakiraman, N., Foon, K. A., Liles, T. M., Dallaire, B. K., Wey, K., Royston, I., Davis, T. and Levy, R. 1997. IDEC-C2B8 (Rituximab) anti-CD20 monoclonal antibody therapy in patients with relapsed low-grade non-Hodgkin's lymphoma. *Blood* 90:2188.
35 Reff, M. E., Carner, K., Chambers, K. S., Chinn, P. C., Leonard, J. E., Raab, R., Newman, R. A. and Hanna, N. 1994. Depletion of B cells *in vivo* by a chimeric mouse human monoclonal antibody to CD20. *Blood* 83:435.
36 Kaminski, M. S., Zasadny, K. R., Francis, I. R., Fenner, M. C., Ross, C. W., Milik, A. W., Estes, J., Tuck, M., Regan, D., Fisher, S., Glenn, S. D. and Wahl, R. L. 1996. Iodine-131-anti-B1 radioimmunotherapy for B-cell lymphoma. *J. Clin. Oncol.* 14:1974.
37 Liu, S. Y., Eary, J. F., Petersdorf, S. H., Martin, P. J., Maloney, D. G., Appelbaum, F. R., Matthews, D. C., Bush, S. A., Durack, L. D., Fisher, D. R., Gooley, T. A., Bernstein, I. D. and Press, O. W. 1998. Follow-up of relapsed B-cell lymphoma patients treated with iodine-131-labeled anti-CD20 antibody and autologous stem-cell rescue. *J. Clin. Oncol.* 16:3270.
38 Tedder, T. F., Klejman, G., Schlossman, S. F. and Saito, H. 1989. Structure of the gene encoding the human B lymphocyte differentiation antigen CD20 (B1). *J. Immunol.* 142:2560.
39 Koller, B. H. and Smithies, O. 1989. Inactivating the β_2-microglobulin locus in mouse embryonic stem cells by homologous recombination. *Proc. Natl Acad. Sci. USA* 86:8932.
40 Zhou, L.-J., Smith, H. M., Waldschmidt, T. J., Schwarting, R., Daley, J. and Tedder, T. F. 1994. Tissue-specific expression of the human CD19 gene in transgenic mice inhibits antigen-independent B lymphocyte development. *Mol. Cell. Biol.* 14:3884.
41 Kearney, J. F., Radbruch, A., Liesegang, B. and Rajewsky, K. 1979. A new mouse myeloma cell line that has lost immunoglobulin expression but permits the construction of antibody-secreting hybrid cell lines. *J. Immunol.* 123:1548.
42 Fujimoto, M., Bradney, A. P., Poe, J. C., Steeber, D. A. and Tedder, T. F. 1999. Modulation of B lymphocyte antigen receptor signal transduction by a CD19/CD22 regulatory loop. *Immunity* 11:191.
43 Bradbury, L. E., Kansas, G. S., Levy, S., Evans, R. L. and Tedder, T. F. 1992. The CD19/CD21 signal transducing complex of human B lymphocytes includes the target of antiproliferative antibody-1 and Leu-13 molecules. *J. Immunol.* 149:2841.
44 Fujimoto, M., Poe, J. C., Jansen, P. J., Sato, S. and Tedder, T. F. 1999. CD19 amplifies B lymphocyte signal transduction by regulating Src-family protein tyrosine kinase activation. *J. Immunol.* 162:7088.
45 Leveille, C., Al-Daccak, R. and Mourad, W. 1999. CD20 is physically and functionally coupled to MHC class II and CD40 on human B cell lines. *Eur. J. Immunol.* 29:65.
46 Engel, P., Zhou, L.-J., Ord, D. C., Sato, S., Koller, B. and Tedder, T. F. 1995. Abnormal B lymphocyte development, activation and differentiation in mice that lack or overexpress the CD19 signal transduction molecule. *Immunity* 3:39.
47 Jacob, R., Kassir, R. and Kelsoe, G. 1991. *In situ* studies of the primary immune response to (4-hydroxy-3-nitrophenyl)acetyl. I. The architecture and dynamics of responding cell populations. *J. Exp. Med.* 173:1165.
48 Takahashi, Y., Dutta, P. R., Cerasoli, D. M. and Kelsoe, G. 1998. In situ studies of the primary immune response to (4-hydroxy-3-nitrophenyl)acetyl. V. Affinity maturation develops in two stages of clonal selection. *J. Exp. Med.* 187:885.
49 Loder, F., Mutschler, B., Ray, R. J., Paige, C. J., Sideras, P., Torres, R., Lamers, M. C. and Carsetti, R. 1999. B cell development in the spleen takes place in discrete steps and is determined by the quality of B cell receptor-derived signals. *J. Exp. Med.* 190:75.
50 Genot, E. M., Meier, K. E., Licciardi, K. A., Ahn, N. G., Uittenbogaart, C. H., Wietzerbin, J., Clark, E. A. and Valentine, M. A. 1993. Phosphorylation of CD20 in cells from a hairy cell leukemia cell line. Evidence for involvement of calcium/calmodulin-dependent protein kinase II. *J. Immunol.* 151:71.
51 Carsetti, R., Köhler, G. and Lamers, M. C. 1995. Transitional B cells are the target of negative selection in the B cell compartment. *J. Exp. Med.* 181:2129.
52 Liang, Y. and Tedder, T. F. 2001. Identification of a CD20, FcεRIβ and HTm4 related gene family. Sixteen new MS4A family members expressed in human and mouse. *Genomics* 72:119.
53 Liang, Y., Buckley, T. R., Tu, L., Langdon, S. D. and Tedder, T. F. 2001. Structural organization of the human MS4A gene cluster on chromosome 11q12: twelve members of the CD20, FcεRIβ and HTm4 gene family. *Immunogenetics* 53:357.
54 Genot, E., Valentine, M. A., Degos, L., Sigaux, F. and Kolb, J. P. 1991. Hyperphosphorylation of CD20 in hairy cells. Alteration by low molecular weight B cell growth factor and IFN-alpha. *J. Immunol.* 146:870.
55 Valentine, M. A., Meier, K. E., Rossie, S. and Clark, E. A. 1989. Phosphorylation of the CD20 phosphoprotein in resting B lymphocytes: regulation by protein kinase C. *J. Biol. Chem.* 264:11282.
56 Valentine, M. A., Licciaradi, K. A., Clark, E. A., Krebs, E. G. and Meier, K. E. 1993. Insulin regulates serine/threonine phosphorylation in activated human B lymphocytes. *J. Immunol.* 150:96.
57 Oettgen, H. C., Bayard, P. J., Van Ewijk, W., Nadler, L. M. and Terhorst, C. P. 1983. Further biochemical studies of the human B-cell antigens B1 and B2. *Hybridoma* 2:17.
58 Deans, J. P., Kalt, L., Ledbetter, J. A., Schieven, G. L., Bolen, J. B. and Johnson, P. 1995. Association of 75/80-kDa phosphoproteins and the tyrosine kinases Lyn, Fyn, and Lck with the B cell molecule CD20. Evidence against involvement of the cytoplasmic regions of CD20. *J. Biol. Chem.* 270:22632.
59 Chu, P. G., Chen, Y.-Y., Molina, A., Arber, D. A. and Weiss, L. M. 2002. Recurrent B-cell neoplasms after Rituximab therapy: an immunophenotypic and genotypic study. *Leuk. Lymph.* 43:2335.